# Magnetic properties of Co/Pt multilayers deposited on silicon dot arrays

S. Landis,* B. Rodmacq, and B. Dieny
*Département de Recherche Fondamentale sur la Matière Condensée, SP2M/Laboratoire Nanostructures et Magnétisme, CEA Grenoble, 17 Avenue des Martyrs, 38054 Grenoble Cédex, France*
(Received 12 May 2000)

Arrays of silicon dots down to 200 nm in size have been prepared by standard lithography and etching techniques, and then covered by different ($Co_{0.5\ nm}/Pt_{1.8\ nm}$) multilayers which exhibit perpendicular magnetic anisotropy. On unpatterned substrates, the coercive field varies between 120 and 400 Oe, depending on the buffer thickness and on the number of layers. Magnetic force microscopy (MFM) images show magnetic domains about 1.2 $\mu$m in size. Deposition of these multilayers on patterned silicon substrates shows that the profile of the magnetic dots is the same as the initial Si dot profile even when the amount of magnetic material represents 60% of the dot height. Atomic force microscopy cross sections indicate that a negligible amount of material is deposited on the side walls of the dots. MFM images of arrays with a dot spacing large enough to explore the bottom of the grooves show that the magnetic domains in areas between the dots are of the same size as on the unpatterned area, although their coercive field is increased from 170 to 300 Oe. On the top of the dots, single-domain configurations are observed, and the coercive field of the dots ranges from 1600 to 2400 Oe. This distribution of switching fields, which only weakly depends on the dot size, is mainly related to the detailed shape of the dots (in particular the sharpness of the corners) and not to their magnetostatic interaction. This confers to each individual dot a well-defined coercive field. The magnetization reversal of a given dot weakly influences its first neighbors, which means that the dots are essentially independent of each other for the range of Co and Pt thickness used in this study. In the same way, no significant coupling is mediated by the continuous magnetic layer in the bottom of the grooves. These results are confirmed by micromagnetic calculations of the magnetic dot-dot and dot-groove interactions for the various geometries that we have investigated.

## I. INTRODUCTION

The fabrication of arrays of submicronic magnetic dots with a well-controlled geometry is very interesting from a fundamental point of view as well as for potential technological applications in ultrahigh-density data storage and integrated magnetoelectronic devices.[1–3] Various properties are investigated in these materials (mechanism of magnetization reversal, domain configurations, coupling between dots, collective excitations, or dipolar effects[4]). Most of the conventional approaches for the preparation of these arrays consist in first depositing the magnetic material on a flat wafer and locally etching it.[4–8] In this paper, we report on the magnetic properties of arrays of dots prepared by another approach which consists in depositing the magnetic film on an array of square Si dots.[9] Such a technique has been previously used for magneto-optic media with, however, dot sizes and separations larger than the ones used in the present study.[10–12]

This method offers a number of advantages: (i) the deposition of the metallic film is the last step of the process, thus eliminating any possible deterioration of its magnetic properties during patterning; (ii) etching of silicon is a very well-controlled technique in microelectronics, thus allowing to prepare magnetic submicrostructures with very high resolution (down to 50 nm), high aspect ratio, and quality; (iii) the substrate preparation is independent of the choice of the magnetic material; therefore, there is no need to find a particular etching procedure for each element. However, the magnetic material is here deposited on the whole substrate. Thus it is important to determine, as a function of both height and separation of the dots, to what extent the amount of material deposited in the grooves separating the dots can modify their magnetic behavior, as compared to the case of patterned magnetic layers.

In this paper, we present results obtained on (Co/Pt) multilayers with perpendicular magnetic anisotropy. The domain structures and the mechanism of the magnetization reversal of the material deposited on the dots and in the grooves are investigated with a magnetic force microscopy (MFM) tip. The switching field distribution of the dots is determined and its width is compared to the magnetostatic coupling between the dots. Finally, micromagnetic calculations of the magnetostatic energy in arrays of various geometries are carried out and compared to experimental results.

## II. SAMPLE PREPARATION

The 8-in. silicon wafers are patterned in the form of arrays of Si square dots by conventional lithographic and etching techniques at LETI in CEA-Grenoble. The different steps involved in the sample preparation are summarized in Fig. 1(a). A 600 nm film of positive resist (UV3 by Shipley) is first deposited on the silicon wafer (step 1) and parallel lines in two orthogonal directions are insulated on the resist with a scanning electron beam. After revelation of the insulated area, an array of resist dots is obtained (step 2). Reactive ion etching then transfers the resist pattern onto the silicon sub-

 

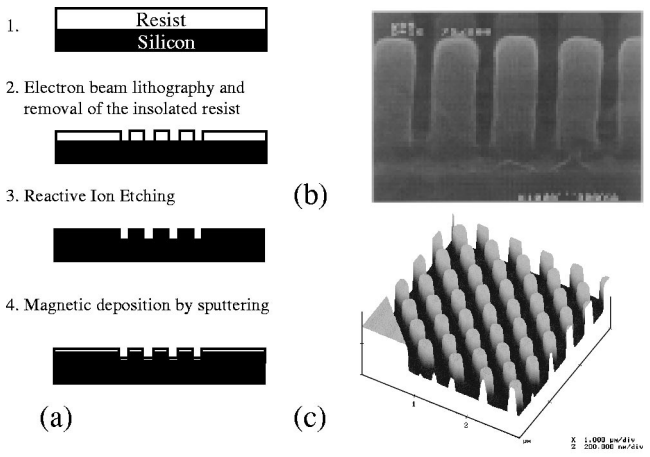


FIG. 1. (a) Lithographic preparation process, (b) scanning electron microscopy image of a (200/75/600) resist dots array, and (c) 3 $\mu$m x 3 $\mu$m AFM image of a (200/200/150) square Si dots array.

strate (step 3). The last step of the preparation consists in sputter-depositing a Co/Pt multilayer on the whole substrate (step 4). Figure 1(b) is a scanning electron microscopy image of the resist array before the silicon etching and Fig. 1(c) is an atomic force microscopy (AFM) image of the silicon array at the end of the patterning process. This figure shows the nice regularity of the arrays. In Fig. 1(c), the dots look cylindrical rather than square. However, this is an artifact of the AFM measurement technique. Due to the size of the AFM tip, the corners of the dots look much rounder than they actually are.

The Si dots used in the present study will be identified in the rest of this paper by $(L/d/h)$, where $L$ is the size of the square dots (from 200 to 400 nm), $d$ is their spacing (100 or 200 nm), and $h$ is their height (47 or 200 nm). The characteristics of the arrays investigated in this study are listed in Table I. On each wafer, six different patterned patches corresponding to various dot sizes were insulated, each patch having a size of 1 mm$\times$30 $\mu$m. For some experiments (magnetization measurements and statistical analysis) larger arrays (3 mm$\times$3 mm) were also prepared.

Co/Pt multilayers exhibit a magnetic anisotropy perpendicular to the film plane.[13–15] Three different multilayers were studied: $Si/SiO_2/Pt_{20nm}/(Co_{0.5\ nm}/Pt_{1.8\ nm})_4$, $Si/SiO_2/Pt_{1.8\ nm}/(Co_{0.5\ nm}/Pt_{1.8\ nm})_4$ and $Si/SiO_2/Pt_{1.8\ nm}/(Co_{0.5\ nm}/Pt_{1.8\ nm})_3$. In all cases the deposition was carried out at room temperature by dc sputtering for cobalt and platinum at a rate of about 0.1 nm/s. The $SiO_2$ layer is the native oxide layer 1 nm thick.

AFM measurements allowed us to determine the rms roughness of the film on the top of the dots, on the continuous layer in the bottom of the grooves, and on the unpatterned area. In all cases we found a roughness of about 0.8 nm.

TABLE I. Structural parameters of the arrays. The numbers give the size $L$, spacing $d$, and height $h$ of the dots in nm, respectively.

| Array |
|---|
| 400/100/47 |
| 400/100/200 |
| 300/100/47 |
| 200/100/200 |
| 200/200/47 |

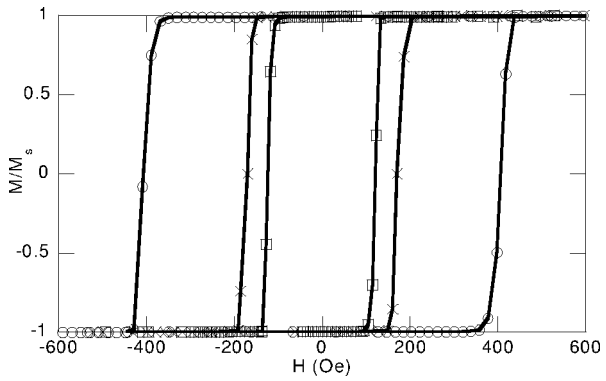


FIG. 2. Hysteresis loops of $Pt_{1.8\ nm}/(Co_{0.5\ nm}/Pt_{1.8\ nm})_3$ (squares), $Pt_{1.8\ nm}/(Co_{0.5\ nm}/Pt_{1.8\ nm})_4$ (crosses), and $Pt_{20\ nm}/(Co_{0.5\ nm}/Pt_{1.8\ nm})_4$ (circles) multilayers, obtained from extraordinary Hall effect measurements. The coercive fields are 120 Oe, 170 Oe, and 400 Oe, respectively.

## III. MAGNETIC PROPERTIES OF Co/Pt MULTILAYERS ON FLAT WAFERS

Figure 2 presents the normalized hysteresis loops of the three multilayers when deposited on unpatterned silicon substrates, the magnetic field being applied perpendicular to the plane of the wafer. They have been obtained from extraordinary Hall effect measurements[16,17] performed at room temperature in the Van der Pauw configuration. In ordinary ferromagnetic samples, the field dependence of the Hall resistivity is given by $\rho_{x,y}(H)=R_0H+4\pi R_sM(H)$, where $R_0$ and $R_s$ are the ordinary and extraordinary Hall coefficients, respectively, and $M(H)$ is the sample magnetization perpendicular to the plane. In the present samples, the ordinary term is very small, and the Hall measurement gives a signal proportional to the magnetization. The square hysteresis loops in Fig. 2 indicate that the magnetization reversal occurs first by nucleation of a reversed domain followed by rapid domain wall motion.[18]

By adjusting the platinum buffer layer thickness or by modifying the number of bilayers, the coercive field can be tuned in a wide range between 100 and 1000 Oe. Honda *et al.*[19] have studied the magnetization process in sputtered (Co/Pt) multilayers. The Co layer thickness was 0.5 nm and the Pt layer thickness was between 0.5 and 1.5 nm, for a number of bilayers between 5 and 60. Their numerical calculations showed that the magnetization process can be approximated by that of a single film having the same characteristics as the multilayer after averaging over its whole thickness. Therefore, our multilayers can be considered as single layers with average magnetization. A vibrating sample magnetometer (VSM) loop with the field applied in the plane of the sample gives an in-plane saturation field $H_s$ of 8500 Oe and a spontaneous magnetization $M_s$ of about 300 emu cm$^{-3}$. From $H_s$ and $M_s$, the effective anisotropy con-

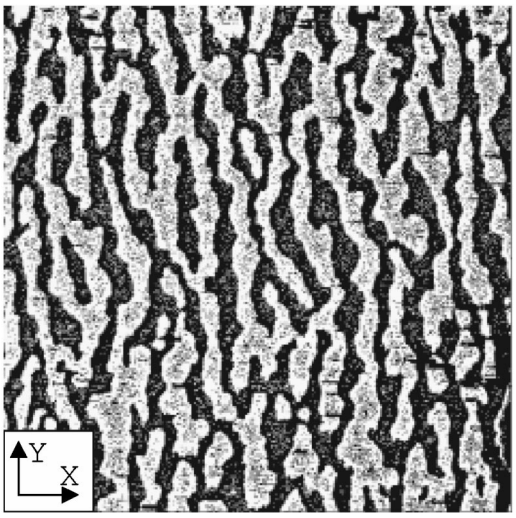


FIG. 3. 40 $\mu$m$\times$40 $\mu$m MFM image of a $Pt_{1.8\ nm}/(Co_{0.5\ nm}/Pt_{1.8\ nm})_4$ multilayer on a flat Si substrate in the demagnetized state.

stant $K_{eff}$ can be calculated using $H_s=2K_{eff}/M_s$, which leads to $K_{eff}=K_u-2\pi M_s^2=1.27\times10^6$ erg cm$^{-3}$. This implies a quality factor $Q=K_u/2\pi M_s^2=3.2$ which is comparable to values found in the literature.[13]

Magnetic imaging of these samples was performed by MFM using a Digital Instrument 3a Nanoscope, with a silicon tip coated with a CoCr film, in Tapping Mode.

The imaging was carried out with a two-step Lift Mode process, the first scan being used to determine the topography and the second one passing at a fixed height above the known surface while recording the magnetic response of the tip with a phase detection system. During the imaging, the tip was magnetized in the direction perpendicular to the sample surface, so that it can roughly be considered as a magnetic dipole. Figure 3 shows an example of the magnetic domain configuration obtained by MFM on a continuous $Pt_{1.8\ nm}/(Co_{0.5\ nm}/Pt_{1.8\ nm})_4$ film. The sample has been demagnetized by rotating it in a static field of decreasing amplitude around the *Y* axis in Fig. 3. This axis is in the plane of the film and perpendicular to the applied field.

Figure 3 shows elongated magnetic domains parallel to the rotation axis with a width of about 1.2 $\mu$m. This anisotropy axis is not characteristic of the magnetic material but is due to the method used to demagnetize the sample. Indeed, when there is a nucleation event, the domain in the *X* direction is subjected to an alternative field. Therefore it cannot expand through the whole sample and reaches an equilibrium size. In contrast, no magnetic field is applied in the *Y* direction. So the domains can keep on growing in this direction during the demagnetization process. This explains why the magnetic domains are elongated in the *Y* direction parallel to the rotation axis. We have performed the same experiment to determine the domain size for 5 samples with a total thickness varying from 11.2 nm (4 bilayers) to 48.8 nm (20 bilayers). Using the relation established by Kaplan and Gehring[20] between the thickness *t* of the film and the domain size d for stripe magnetic domains,

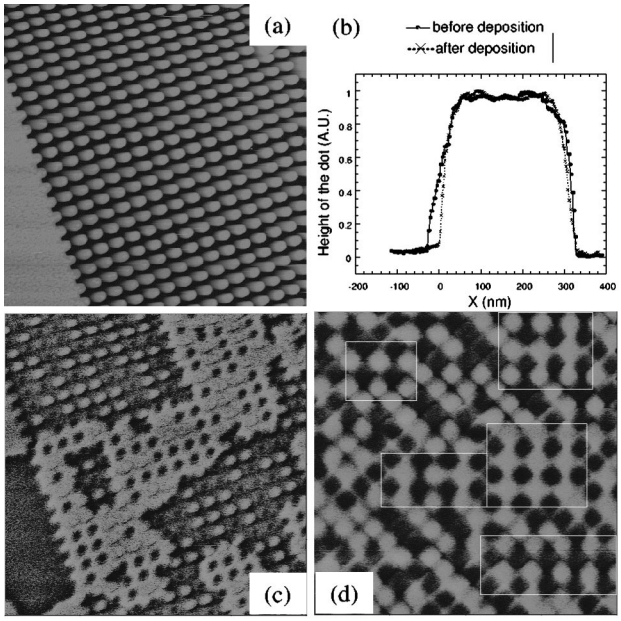


FIG. 4. (a) 8 $\mu$m$\times$8 $\mu$m AFM image of a $Pt_{20\ nm}/(Co_{0.5\ nm}/Pt_{1.8\ nm})_4$ multilayer on a (200/200/47) array, (b) AFM cross section of a dot before and after deposition of the multilayer, (c) 8 $\mu$m$\times$8 $\mu$m MFM image of the same array, (d) 8 $\mu$m$\times$8 $\mu$m MFM image of a (400/100/47) array coated with the same multilayer. Local checkerboard pattern are shown in white boxes.

$$d=t\exp\left[\frac{\pi D_0}{2t}\right]\exp\left[1+\frac{\pi b}{2}\right],$$

where $b$ is a constant equal to $-0.66$ and $D_0$ the characteristic dipolar length, we determine $D_0=\sigma_w/2\pi M_s^2=41$ nm, which gives for the wall energy $\sigma_w=2.3$ erg cm$^{-2}$. The domain wall (Bloch wall) width can thus be determined by $l=\sigma_w/4K_u=3.1$ nm.

## IV. ARRAYS OF (Co/Pt) SUBMICRONIC DOTS

The arrays studied in this section are (200/200/47) and (400/100/47) ones on which a $Pt_{20\ nm}/(Co_{0.5\ nm}/Pt_{1.8\ nm})_4$ multilayer has been deposited. The AFM image of the first sample [Fig. 4(a)] reveals that the magnetic deposit does not modify the topography of the sample and that the dots are still well defined after the deposition of 29.2 nm material, which represents more than 60% of the initial dot height. Figure 4(b) is an AFM cross section of one dot of this array. Although the image is the convolution of the real dot profile and of the tip shape (leading to nonvertical dot walls), it is possible to study the evolution of the height and width of the dot after the deposition of the multilayer. Neither the height nor the width of the dots is modified, meaning that the profile is perfectly reproduced after deposition. In other words, it seems reasonable to assume that no significant amount of magnetic material is present on the side walls of the dots. This assumption will be used in the micromagnetic calculations presented in Sec. VII. Electron microscopy experiments are underway in order to analyze these profiles with a much higher resolution.

Figure 4(c) shows the corresponding magnetic image of

the same array in the as-deposited state (i.e., without any magnetic treatment). A uniform white or dark contrast is seen on each dot, which indicates that the dots are single domain. All sizes investigated (400, 300 and 200 nm) led to the same observation. The spacing of 200 nm between dots allows the tip to explore the magnetic configuration in the bottom of the grooves. The continuous magnetic medium within the grooves has a domain size of about 3–4 $\mu$m, comparable to the one observed on the flat part of the wafer (bottom left of the image). In this figure, it also appears that the magnetization of the dots can be up or down whatever the magnetization direction in the grooves. This shows that there is no significant direct exchange coupling between the magnetic material at the top of the dots and in the grooves via the magnetic deposit which may exist on the sidewalls of the dots. This confirms that if any magnetic deposit is present on the walls, its thickness must be much smaller than the nominal one.

Figure 4(d) shows the magnetic image of the other array (400/100/47). In this case, the small spacing between the dots (100 nm) prevents the tip from imaging the magnetic configuration in the bottom of the grooves. Local checkerboard patterns are observed on this image. This magnetic configuration corresponds to the minimum of the magnetostatic energy for a square lattice of interacting magnetic particles with perpendicular anisotropy. The absence of such a magnetic correlation on the array with 200 nm spacing [Fig. 4(c)] indicates that the dominant magnetostatic interaction in Fig. 4(d) is the interaction between the top of neighboring dots.

## V. MAGNETIZATION REVERSAL OF THE ARRAYS

In order to assess whether these systems can be used as ultrahigh magnetic recording media, we made some writing tests by using a MFM tip as a local field source as Kleiber *et al.*[21] and Kong *et al.*[22]

As a first step, we studied the magnetization reversal of a $Pt_{1.8\ nm}/(Co_{0.5\ nm}/Pt_{1.8\ nm})_4$ multilayer on the flat part of the substrate (outside the array) in order to determine the magnetic stray field of the MFM tip. We used a 40-nm CoCr-coated tip and the (200/200/47) array in order to be able to also image the magnetic configuration in the bottom of the grooves. The image of Fig. 5(a) was recorded without an external field, and Fig. 5(b) (recorded on the same area but with an applied magnetic field of 35 Oe) shows that only the magnetization on the flat part of the wafer has reversed after several scans. This means that the sum of the stray field from the tip and of the external field of 35 Oe is of the order of the coercive field of the continuous film ($H_c = 170$ Oe as obtained from the Hall experiments). Therefore the magnetic field created by the tip has a magnitude of about 135 Oe, comparable to the values reported in the literature for such MFM tips.[23]

The fact that the magnetic configuration in the grooves is unchanged [Fig. 5(b)] means that, although the material deposited in the bottom of the grooves is continuous, its coercive field is larger than 170 Oe. Figures 5(c) and 5(d) present MFM images obtained with the same tip on another part of the sample. Figure 5(c) shows the magnetic configuration in the as-deposited state. Then successive images were recorded while *in situ* increasing the external magnetic field. Figure 5(d) corresponds to an external field of 170 Oe, that is, a total field of 305 Oe. The magnetization in the bottom of the grooves has now reversed. In contrast, the magnetization on top of the dots is still in the initial direction. We recall that the scans have been recorded in tapping mode. Thus the stray field generated by the tip on the material in the grooves is the same as the one previously determined on the flat part of the wafer, although the grooves are located 47 nm below both the unpatterned area and the top of the dots. One thus obtains a coercive field of about 300 Oe for the magnetic material in the grooves, that is, almost twice the value obtained on the unpatterned area. This enhanced coercivity can be ascribed to the fewer number of nucleation centers (defects) in the grooves and/or to the pinning of the domain walls at the foot of the dots.

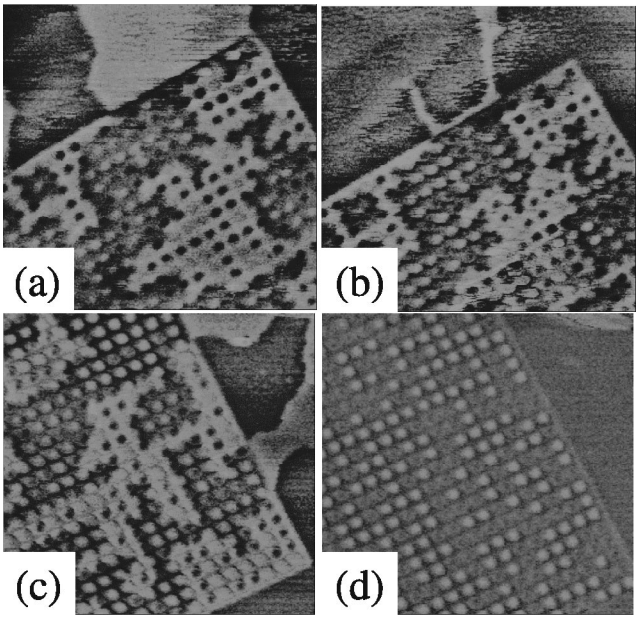


FIG. 5. 6 $\mu$m$\times$6 $\mu$m MFM images of a $Pt_{1.8\ nm}/(Co_{0.5\ nm}/Pt_{1.8\ nm})_4$ multilayer on a (200/200/47) array. Top: without external field (a) and with an applied field of 35 Oe (b). Bottom: another area without external field (c) and with an applied field of 170 Oe (d).

In order to be able to reverse the magnetization of the dots, we used a MFM tip with a higher magnetic moment (a 80-nm CoCr-coated tip) which creates a stronger stray field. Furthermore, we deposited a (Co/Pt) multilayer with only three repeats in order to decrease the coercive field of the continuous layer (120 Oe in this case), assuming that this would also decrease the coercive field of the dots.

For particles with perpendicular anisotropy, the magnetic poles are located all over the surface, and their influence is dominant in the reversal process. The reversal behavior is not very different from that of the continuous film as long as the particle size is well above the domain wall width.[24–26] Here, the domain wall width (3.1 nm) is by far smaller than the dot size, so we can suppose that the magnetization reversal on the dots occurs by nucleation of reversed domains and propagation. The nucleation is expected to take place at the

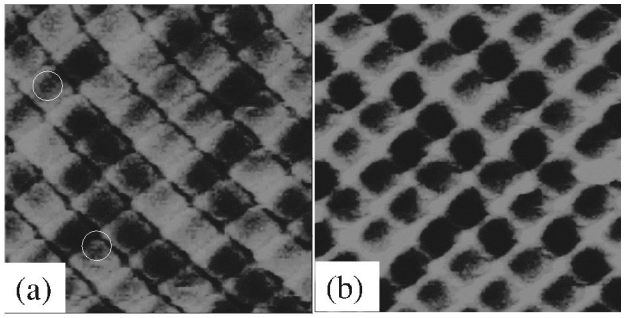


FIG. 6. 4 $\mu$m$\times$4 $\mu$m MFM images (using a 80-nm CoCr-coated tip) of a $Pt_{1.8\ nm}/(Co_{0.5\ nm}/Pt_{1.8\ nm})_3$ multilayer on a (400/100/47) array. Image (a) is the first scan after demagnetization of the sample and image (b) is the same area after several scans.

center of the dots where the demagnetizing field is maximum or at the corner of the dots where the remnant magnetization is the most distorted in the so-called ''flower pattern.''[27] MFM images of a (400/100/47) array corroborate this assumption as can be seen in Fig. 6(a) where the sample was first demagnetized with the same procedure used for continuous multilayers (see previously). The areas with dark contrasts have their magnetization in the down direction (like the tip), whereas white contrasts are associated with a magnetization in the up direction. Using a MFM tip with a high magnetic moment leads to the observation of small dark contrast areas at the center or corners of white dots, as shown by circles in Fig. 6(a). This confirms that the switching of the magnetization does not occur by coherent rotation but by a nucleation-propagation mechanism. Figure 6(b) is an image of the same part of the sample after several scans. The magnetization of all dots has now switched. It must be noted that the white contrasts around the dots result from the stray field of the dots and do not imply that the magnetization at the edge of the dots switched again in the opposite direction.

Recent studies on MFM tips similar to the ones used here indicate local fields larger than 1000 Oe.[28] Thus we can conclude that the coercive field of the dots is larger than 1000 Oe, compared to 300 Oe for the grooves and 170 Oe for the unpatterned area. As in Refs. 29 and 30, the coercive field of the dots is thus strongly enhanced compared to continuous layers. This can be understood by considering that, on a continuous layer in which there is easy wall propagation, the reversal field of the whole sample is extremely dependent on the presence of major defects which act as nucleation centers. For the dots, the domain wall propagation is necessarily stopped at the dot edges. Therefore, the nucleation must take place on every individual dot, leading to a larger reversal field.

## VI. DETERMINATION OF THE SWITCHING FIELD DISTRIBUTION

In this section, we report on the determination of the switching field distribution in these arrays of magnetic dots. Figure 7 shows a sequence of MFM images of a (400/100/200) array coated with a $Pt_{1.8\ nm}/(Co_{0.5\ nm}/Pt_{1.8\ nm})_4$ multilayer. The images were recorded with a 40-nm CoCr-coated tip, giving a stray field ($\simeq$135 Oe) much smaller than the coercive field of the dots ($>$1000 Oe). Between each image, the sample was saturated in a positive field perpendicular to the film plane. Then a negative field $H_{ext}$ was applied and switched off, the MFM measurements being performed in the remnant state. Dots with dark contrasts are still magnetized in the positive saturation direction, whereas the magnetization in the dots with white contrasts has switched in the down direction after the application of $H_{ext}$.

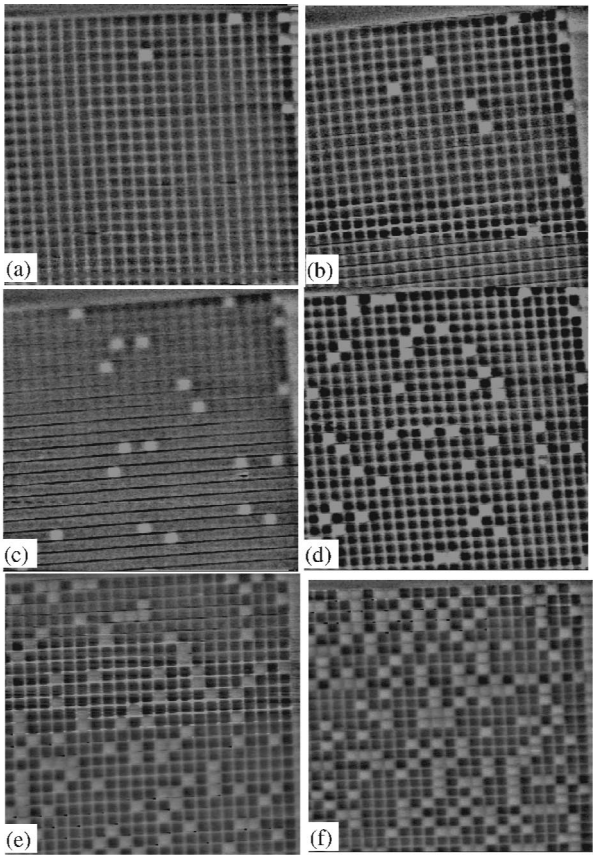


FIG. 7. Sequence of 12 $\mu$m$\times$12 $\mu$m MFM images of a $Pt_{1.8\ nm}/(Co_{0.5\ nm}/Pt_{1.8\ nm})_4$ multilayer on a (400/100/200) array. Between each image, the sample was saturated in a positive field perpendicular to the film plane. Images were recorded in the remnant state after applying an external field $H_{ext}$ perpendicular to the plane and decreasing from $-1400$ (a) to $-1900$ Oe (f) by steps of $-100$ Oe.

Since minor hysteresis loops obtained either from Hall effect (on continuous layers) or from superconducting quantum interference device (SQUID) experiments (on continuous layer and on dot arrays) show that the magnetization is constant when going from $H_{ext}$ to $H=0$, this implies that the magnetic structure (i.e., the proportion of dots with up and down magnetization) is the same under $H_{ext}$ and in the remnant state.

By increasing the negative applied field, it is found that the reversal of the magnetization of the dots takes place between $-1600$ Oe and $-2400$ Oe. This is in agreement with SQUID experiments we carried out on the same sample (a $3\times3$ mm array). This validated our assumption and our experimental process for the determination of the switching field by MFM. Besides, the width of the distribution is com-

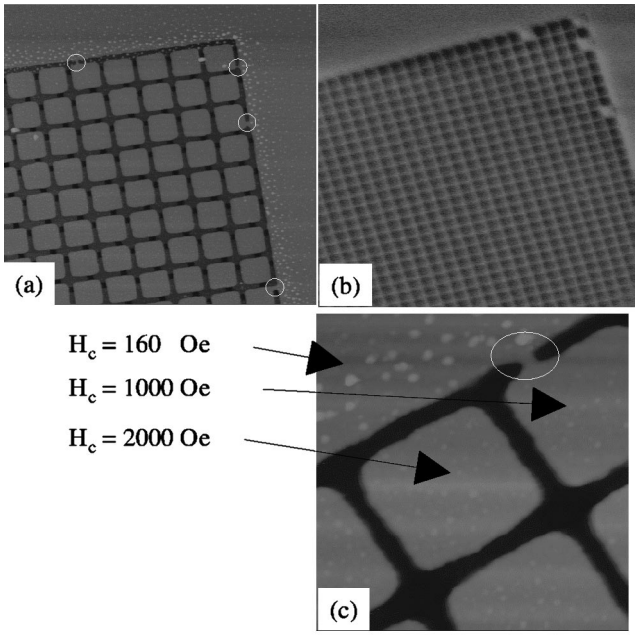


FIG. 8. (a) 5 $\mu$m$\times$5 $\mu$m AFM image of a $Pt_{1.8\ nm}/(Co_{0.5\ nm}/Pt_{1.8\ nm})_4$ multilayer on a (400/100/200) array. The four encircled dots are the first reversed ones. (b) 12 $\mu$m$\times$12 $\mu$m MFM corresponding image, which shows these first four reversed dots. (c) 1 $\mu$m$\times$1 $\mu$m AFM view of image (a) showing a bridge between one of these dots and the unpatterned area.

parable to results obtained by other authors.[31] This width may have two origins: one is the intrinsic switching field distribution of the assembly of dots supposed to be magnetostatically independent of each other; the other is the influence of the magnetostatic interactions between dots which shifts the hysteresis loop of a given dot towards positive or negative fields depending on the magnetic configuration of all the other dots. However, our calculations of magnetostatic coupling (see Sec. VII) show that the maximum magnetostatic field on a given dot, generated by all other dots, is 43 Oe for the array of Fig. 7. This is much lower than the width of the distribution of switching fields which is of the order of 800 Oe. The magnetostatic interaction is therefore a minor contribution to the width of the distribution.

In addition, it is interesting to note that, despite the fact that the sample was saturated in the positive direction between each MFM measurements, the switching sequence is always the same. This means that every given dot has its own coercive field. This property was observed for all arrays we have studied. We think that a large part of the width of the distribution is due to the exact shape of the corners of the dots where the magnetization is the most distorted. Slight fluctuations in this shape may exist from dot to dot which may lead to a strong variation in switching field whenever the nucleation of the magnetization reversal takes place at the corners of the dots.

In order to try to correlate the switching fields with some particular structural defects of the dots, we carried out a detailed AFM study, selecting two particular dots with switching fields at the lower and upper part of the distribution. Unfortunately the resolution of this technique did not allow us to establish a clear correlation between the nanostructure

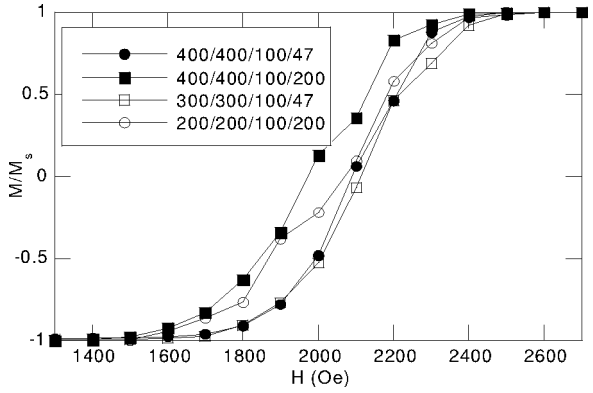


FIG. 9. Half of the hysteresis loops of different arrays calculated from MFM sequences identical to the one of Fig. 7.

of the dots and their switching field.

However, in a particular situation, we have been able to identify the defects responsible for the weak reversal field for four dots near the unpatterned area at the right top part of the array in Fig. 8. AFM images show residual bridges between the flat part of the wafer and the patterned area. The reversal field in the connected dots falls to 1000 Oe compared to about 2000 Oe for isolated dots. Fournel *et al.*[32] showed that the switching field of a dot bridged to a large continuous area rapidly increases when the bridge width decreases but does not depend neither on the bridge length nor on the dot size. The reversal field for these bridged dots is therefore lower than for isolated dots due to the propagation of a domain wall from the continuous area through the bridge. It is, however, higher than on the continuous layer due to the difficulty for the domain wall to propagate through the bridge.

From sequences similar to the one shown in Fig. 7, the hysteresis loop can be calculated by using a relation of the form $M/M_s=(n_\uparrow-n_\downarrow)/(n_\uparrow+n_\downarrow)$, where $n_\uparrow$ and $n_\downarrow$ are the number of dots magnetized either in the up or down direction. Figure 9 shows the positive branch of the loops calculated for different arrays. The average coercive field (Table II) is about 12 times larger than for the continuous film ($H_c=170$ Oe). There is some tendency for the reversal fields to increase with decreasing the dot size, in agreement with results found in the literature.[30,33] However, a relatively weak change in coercive field, less than 10%, is observed between the different samples, although the dot area varies by a factor of 4. This indicates that the reversal mechanism is qualitatively the same for all sizes. Furthermore, this confirms that the nucleation events do not take place on randomly distributed centers on the surface or edges of the dots (which would lead to a strong dependence of the reversal

TABLE II. Average coercive field of dots deduced from the hysteresis loops.

| Array | Average coercive field (Oe) |
|---|---|
| 400/100/200 | 1980 |
| 400/100/47 | 2100 |
| 300/100/47 | 2120 |
| 200/100/200 | 2070 |

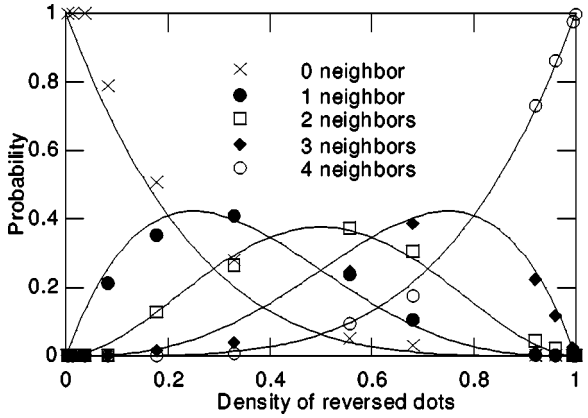


FIG. 10. Probabilities for a given reversed dot to have zero, one, two, three or four first neighbor dots also reversed as a function of the density of reversed dots in the array. Experimental data (symbols) are compared to a binomial law (solid line).

field on the dot size), but rather occur at the center or corners of the dots. In addition, these changes in coercive fields can be quantitatively accounted for by considering the variation of the magnetostatic energy with the size of the dots (see Sec. VII).

Finally from Fig. 7, a statistical analysis of the magnetization reversal of the dots can be performed. In particular, the probability for a given reversed dot to have zero, one, two, three or four first neighbors also reversed can be calculated. These experimental probabilities are compared with the calculated probability assuming that the dots have no correlation between them. Under this assumption, the probability to have $x$ first reversed neighbors as a function of the average density $d$ of reversed dots is given by a binomial law: $P(x)=C_4^x d^x(1-d)^{4-x}$. Figure 10 shows that a good agreement is obtained between experiments and the binomial law. This implies that the dots are essentially uncorrelated, which means that the defects which act as nucleation centers on the dots are randomly distributed all over the array.

## VII. MICROMAGNETIC CALCULATIONS

In this section, we describe the calculation of the magnetostatic energy of these arrays of dots. Our goal is to determine how the coupling between the top of the dots and the bottom of the groove and the coupling between the top of adjacent dots depend on the geometry (dot spacing and dot height) and on the amount of magnetic material. The magnetostatic field generated on a given dot by the rest of the array is also calculated from the magnetostatic energy, and the experimental results are compared to these micromagnetic calculations.

### A. Model

We recall that MFM images [Fig. 4(c)] show that after demagnetizing the sample, the domain size in the grooves is much larger than the dot size. In order to simplify the calculations, we thus consider that the magnetization in the grooves is uniform around a considered dot. Furthermore, we suppose (and we showed in Sec. IV that this was a reasonable assumption) that there is magnetic material only on the

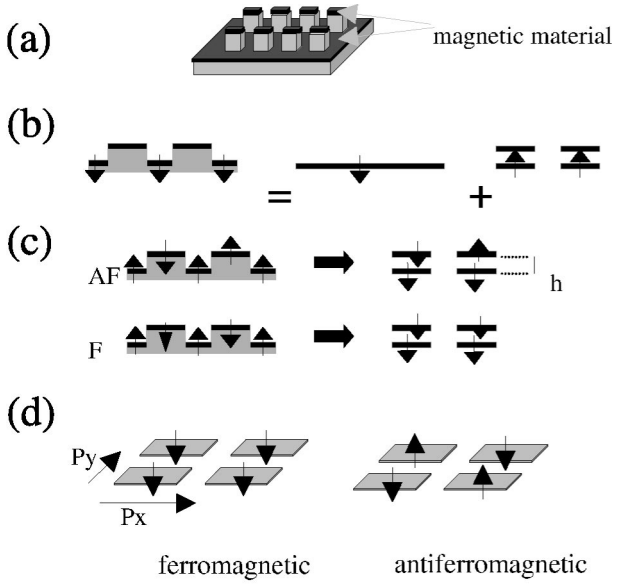


FIG. 11. (a) Schematic representation of the magnetic state of the arrays for the micromagnetic calculations, (b) the superposition principle for the magnetic deposit in the bottom of the grooves, (c) these two magnetic configurations are equivalent to two arrays of dots separated by a height $h$, and (d) magnetic patterns, on four dots, considered in order to determine the magnetic ground state, the ferromagnetic one (left) and the antiferromagnetic one (right).

top of the dots and in the bottom of the grooves but no magnetic deposit is considered on the sidewalls of the dots. We consider an infinite two-dimensional (2D) array of magnetic dots. Several micromagnetic calculations have been previously performed on such arrays.[34–36] The particularity here is the presence of the magnetic material in the grooves which cannot be neglected in the calculation of the magnetostatic energy.

Figure 11(a) schematically shows the structure of the array. According to the superposition principle, the deposit in the grooves can be treated as the sum of an infinite continuous layer, with uniform magnetization, and an array of dots with opposite magnetization [Fig. 11(b)]. The system is therefore equivalent to an infinite continuous layer and two arrays of dots separated by a height $h$. The continuous film only adds a constant contribution to the magnetostatic energy since the stray field outside the layer is equal to zero. In the following we can therefore neglect this contribution to the magnetic energy and only calculate the magnetostatic energy of two arrays of dots separated by a height $h$ [Fig. 11(c)]. To determine for which geometry the coupling between the groove and the top of the dots is less energetic than the coupling between the top of the dots, two magnetic dot patterns have to be considered [Fig. 11(d)]: the ferromagnetic pattern (FP) and the antiferromagnetic one (AFP). In these infinite arrays, the magnetization is a 2D periodic function with periodicities $P_x=2(L_x+d_x)$ and $P_y=2(L_y+d_y)$ along the $X$ and $Y$ axes, respectively, in which $L_x$ and $L_y$ are the dot dimensions and $d_x$ and $d_y$ the dot spacings. It may therefore be expanded as a two-dimensional Fourier series.[37,38]

Considering the multilayer film as a uniform monolayer film of thickness $t$, the magnetization function is for the AFP pattern

$$M_z(x,y)=\sum_{m,n\geqslant 1}^{odd}\frac{16M_s}{mn\pi^2}\sin\left[m\pi\frac{L_x}{P_x}\right]\sin\left[n\pi\frac{L_y}{P_y}\right](-1)^{(m+n)/2-1}\sin\left[2m\pi\frac{x}{P_x}\right]\sin\left[2n\pi\frac{y}{P_y}\right] \tag{1}$$

and for the FP pattern

$$M_z(x,y)=-4M_s\frac{L_xL_y}{P_xP_y}+\sum_{m\geqslant 2}^{even}-\frac{8M_sL_y}{m\pi P_y}\sin\left[m\pi\frac{L_x}{P_x}\right](-1)^{m/2}\cos\left[2m\pi\frac{x}{P_x}\right]+\sum_{n\geqslant 2}^{even}-\frac{8M_sL_x}{n\pi P_x}\sin\left[m\pi\frac{L_y}{P_y}\right](-1)^{n/2}\cos\left[2n\pi\frac{y}{P_y}\right]$$
$$+\sum_{m,n\geqslant 2}^{even}-\frac{16M_s}{mn\pi^2}\sin\left[m\pi\frac{L_x}{P_x}\right]\sin\left[m\pi\frac{L_y}{P_y}\right](-1)^{(m+n)/2}\cos\left[2m\pi\frac{x}{P_x}\right]\cos\left[2n\pi\frac{y}{P_y}\right]. \tag{2}$$

By solving the Poisson equation $\nabla^2\phi=4\pi\nabla\vec{M}$, the potential $\phi$ can be derived and the magnetostatic energy can be calculated using $E=\frac{1}{2}\mu_0\int_S\phi(r)\sigma(r)d^2r$, where $\sigma$ is the surface density of magnetic poles ($\sigma=\vec{M}\cdot\vec{n}$, $\vec{n}$ normal to the plane) and $S$ the dot area. For an infinite array of dots in the antiferromagnetic configuration, this energy is

$$E_{AF}=\mu_0M_s^2\sum_{m,n\geqslant 1}^{odd}\frac{32}{(mn)^2\pi^5\sqrt{\left(\frac{m}{P_x}\right)^2+\left(\frac{n}{P_y}\right)^2}}\sin^2\left[m\pi\frac{L_x}{P_x}\right]\sin^2\left[n\pi\frac{L_y}{P_y}\right]$$
$$\times\sinh\left[\pi t\sqrt{\left(\frac{m}{P_x}\right)^2+\left(\frac{n}{P_y}\right)^2}\right]\exp\left[-\pi t\sqrt{\left(\frac{m}{P_x}\right)^2+\left(\frac{n}{P_y}\right)^2}\right]. \tag{3}$$

If $L_x=P_x/2$ and $L_y=P_y/2$, Eq. (3) gives the dipolar energy calculated by Kaplan and Gehring[20] for the checkerboard pattern. In the same way, if $P_y$ tends to infinity, Eq. (3) leads to the dipolar energy of a stripe pattern.[20]

Similarly, the magnetostatic energy for an infinite arrays of dots in the ferromagnetic configuration is

$$E_F=8t\mu_0M_s^2\left(\frac{L_xL_y}{P_xP_y}\right)^2+\mu_0M_s^2\sum_{m\geqslant 2}^{even}\frac{16P_xL_y^2}{(m\pi)^3P_y^2}\sin^2\left[m\pi\frac{L_x}{P_x}\right]\sinh^2\left[m\pi\frac{t}{P_x}\right]\exp\left[-m\pi\frac{t}{P_x}\right]$$
$$+\mu_0M_s^2\sum_{n\geqslant 2}^{even}\frac{16P_yL_x^2}{(n\pi)^3P_x^2}\sin^2\left[n\pi\frac{L_y}{P_y}\right]\sinh^2\left[n\pi\frac{t}{P_y}\right]\exp\left[-n\pi\frac{t}{P_y}\right]$$
$$+\mu_0M_s^2\sum_{m,n\geqslant 2}^{even}\frac{32\sin^2\left[m\pi\frac{L_x}{P_x}\right]\sin^2\left[n\pi\frac{L_y}{P_y}\right]}{(mn)^2\pi^5\sqrt{\left(\frac{m}{P_x}\right)^2+\left(\frac{n}{P_y}\right)^2}}\sinh\left[\pi t\sqrt{\left(\frac{m}{P_x}\right)^2+\left(\frac{n}{P_y}\right)^2}\right]\exp\left[-\pi t\sqrt{\left(\frac{m}{P_x}\right)^2+\left(\frac{n}{P_y}\right)^2}\right]. \tag{4}$$

For the calculation of the magnetostatic interaction energy between the two arrays of dots separated by a height $h$, only the case of the ferromagnetic pattern must be considered. Indeed, for the antiferromagnetic case, the product of the potential $\phi$ generated by one array and the surface density $\sigma$ of the other array is an odd function. As a result, the double integration for the calculation of $E$ leads to an even function which gives no contribution to the magnetostatic energy. So for two arrays with a thickness $t$ of magnetic material in the ferromagnetic configuration and separated by a height $h$, the magnetostatic interaction energy is

$$E_{int}=\mu_0M_s^2\sum_{m\geqslant 2}^{even}\frac{16P_xL_y^2}{(m\pi)^3P_y^2}\sin^2\left[m\pi\frac{L_x}{P_x}\right]\sinh^2\left[m\pi\frac{t}{P_x}\right]\exp\left[-m2\pi\frac{h}{P_x}\right]$$
$$+\mu_0M_s^2\sum_{n\geqslant 2}^{even}\frac{16P_yL_x^2}{(n\pi)^3P_x^2}\sin^2\left[n\pi\frac{L_y}{P_y}\right]\sinh^2\left[n\pi\frac{t}{P_y}\right]\exp\left[-n2\pi\frac{h}{P_y}\right]$$
$$+\mu_0M_s^2\sum_{m,n\geqslant 2}^{even}\frac{32\sin^2\left[m\pi\frac{L_x}{P_x}\right]\sin^2\left[n\pi\frac{L_y}{P_y}\right]}{(mn)^2\pi^5\sqrt{\left(\frac{m}{P_x}\right)^2+\left(\frac{n}{P_y}\right)^2}}\sinh\left[\pi t\sqrt{\left(\frac{m}{P_x}\right)^2+\left(\frac{n}{P_y}\right)^2}\right]\exp\left[-2\pi h\sqrt{\left(\frac{m}{P_x}\right)^2+\left(\frac{n}{P_y}\right)^2}\right]. \tag{5}$$

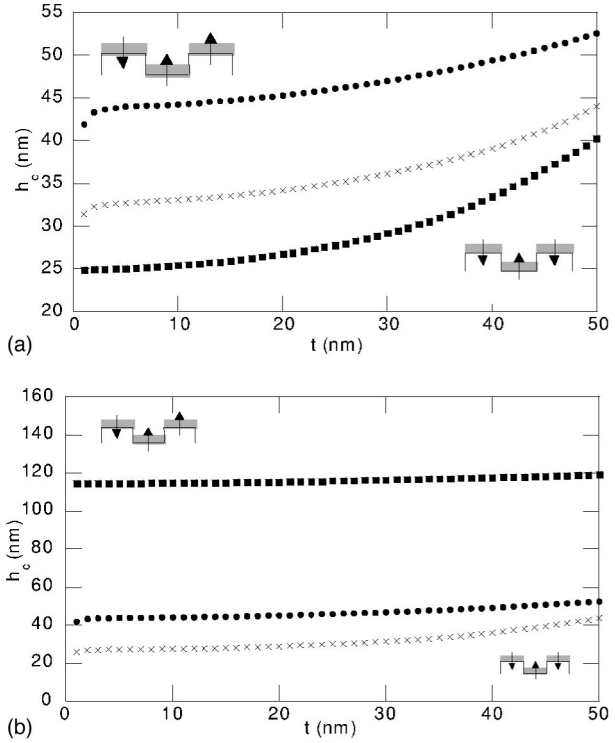


FIG. 12. (a) Magnetostatic phase diagram ($h_c$, $t$) for dot sizes of 400 nm (squares), 300 nm (crosses), and 200 nm (circles) with a spacing of 100 nm; (b) same diagram for a dot size of 200 nm and spacings of 200 nm (squares), 100 nm (circles), or 75 nm (crosses).

Therefore, from Fig. 11(c), the magnetostatic energy is $E^{AF}=E_{AF}+E_F$ for the antiferromagnetic configuration and $E^F=E_{int}+2E_F$ for the ferromagnetic configuration. Furthermore, the magnetostatic field acting on a given dot and generated by all other dots and by the magnetic material in the grooves can be obtained by using $\vec{H}=-\vec{\nabla}\phi$. The dependence of this magnetostatic field on the geometry of the arrays can thus be investigated.

### B. Magnetostatic phase diagram

As mentioned before, the magnetic material in the grooves may induce a magnetostatic coupling between the top of the dots and the bottom of the grooves. So in order to determine which configuration (FP or AFP) has the minimum magnetostatic energy as a function of $L_x$, $d_x$, $L_y$, $d_y$, $h$, and $t$, the equation $E_{int}+E_F-E_{AF}=0$ must be solved. To reduce the numbers of variables, we fix the size of the dots ($L_x$ and $L_y$) and their spacing ($d_x$ and $d_y$) and determine the values of the thickness $t$ and critical height of dots $h_c$, for which the two configurations have the same energy. Figure 12 gives the variation of $h_c$ as a function of the thickness $t$ of magnetic material for dots of different sizes and a constant spacing of 100 nm [Fig. 12(a)] and for 200 nm dots with different spacings [Fig. 12(b)]. The first point to note is that for a fixed thickness and for large values of $h$, the configuration of lowest magnetostatic energy is the antiferromagnetic pattern (checkerboard pattern). This can be easily understood by considering that in this case the dominant interaction is the magnetostatic interaction between the top of the dots. This is also the most stable configuration for all arrays which have no magnetic material around the dots.[4] Conversely, for small values of $h$, the ferromagnetic pattern is less energetic than the antiferromagnetic one. The dots are therefore coupled by dipolar interactions with the bottom of the grooves [the second case in Fig. 11(c)].

TABLE III. Maximum magnetostatic field created by the array on a given dot.

| Array | Maximum magnetostatic field (Oe) |
|---|---|
| 400/100/200 | 70 |
| 400/100/47 | 43 |
| 300/100/47 | 88 |
| 200/100/200 | 42 |
| 200/100/47 | 115 |

To compare these calculations with the experimental results, we have demagnetized the (400/100/200) array. By using six images (18 $\mu$m$\times$18 $\mu$m each) taken from a 3 mm$\times$3 mm array, we have then imaged the magnetic configuration by MFM over an area of about 8000 dots, and determined by statistical analysis the correlation coefficient $R$ between two first-neighbor dots. This coefficient reflects the magnetization alignment between adjacent dots, and ranges from $-1$ for an antiferromagnetic alignment (checkerboard pattern) to $+1$ for a ferromagnetic alignment. For this array, $R$ is found equal to $-0.35$ which reveals that there is a real tendency towards an antiferromagnetic alignment between neighboring dots. The micromagnetic calculations [Fig. 12(a)] show that, for this array, the antiferromagnetic pattern has a lower energy than the ferromagnetic one, which favors the antiferromagnetic alignment between adjacent dots. Therefore, this experiment agrees with the micromagnetic calculations. It should be noted that if $R$ is not equal to $-1$, it is essentially due to the difficulty to reach the demagnetized state of lowest magnetostatic energy in these arrays. Indeed, we saw before that the distribution of switching fields in such arrays is determined by the distribution of nucleation centers, which is random. Therefore the demagnetized state reached here is a metastable configuration but not the one of lowest energy for which $R$ would be equal to $-1$.

### C. Magnetostatic and pinning energy

In the prospect of using such arrays as magnetic storage media, it is important to check the stability of any written magnetic configuration against magnetostatic interactions between dots. Therefore calculations of the maximum magnetostatic field on a given dot were made and compared to the coercive field. This magnetostatic field corresponds to the one created by the whole array on a given dot. From the magnetostatic phase diagram and the five geometries listed in Table I, this field is maximum when the magnetization of all dots and of the magnetic deposit in the grooves are parallel. In Table III, the calculated fields are listed for the different geometries. A maximum field of 115 Oe is found for the (200/200/47) array, lower than the coercive field in the continuous layer (170 Oe) and therefore by far lower than the reversal field of the dots (1600–2400 Oe) determined by SQUID and MFM measurements.

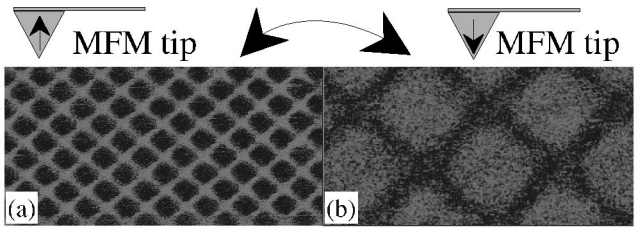


FIG. 13. MFM images in the remnant state after saturation along the normal to the film plane of a $Pt_{20\ nm}/(Co_{0.5\ nm}/Pt_{1.8\ nm})_4$ multilayer on a (400/100/47) array: (a) 5 $\mu$m$\times$2.5 $\mu$m image with the MFM tip saturated along the up direction; (b) 1.5 $\mu$m$\times$0.75 $\mu$m image with the MFM tip saturated along the opposite direction.

MFM experiments were also carried out to confirm the relatively weak value of the magnetostatic energy compared to the pinning one. The sample was first saturated along the normal to the film plane and MFM scans were performed in the remnant state (Fig. 13). Imaging the same array with a MFM tip saturated in the opposite direction leads to the same type of image, although with reversed contrasts. This demonstrates that all contrasts in Fig. 13 only originate from the magnetization of the sample. Furthermore, it appears that this saturated magnetic configuration, which is the configuration of highest magnetostatic energy, is stable in time at room temperature for several days. So the pinning energy in the dots is much higher than the magnetostatic energy. As a consequence, any magnetic configuration could be stored in these arrays.

### D. Influence of the geometry on the coercive field

We mentioned above that the coercive field of the dots was only weakly dependent on the different geometries of the arrays (Fig. 9). Actually these variations can be entirely accounted for by the variation of the magnetostatic energy due to the variation of the dots size and spacing. For two arrays with different geometries, the field on a given dot is different because of three contributions: (i) as the distance between dots varies, the field created by all the other dots is modified; (ii) in addition the field generated by the magnetic deposit in the bottom of the grooves varies with the spacing between dots; (iii) finally, the *z* component of the demagnetizing field inside the dot is reduced when the dot size decreases. As we want to determine the change in coercive field of the whole array, the average magnetization of the dots is assumed equal to zero.

In order to estimate the magnitude of the first contribution, we consider an unfavorable magnetic configuration in which all the nearest neighbors of a given dot have their magnetization parallel. Calculation of the magnetostatic field

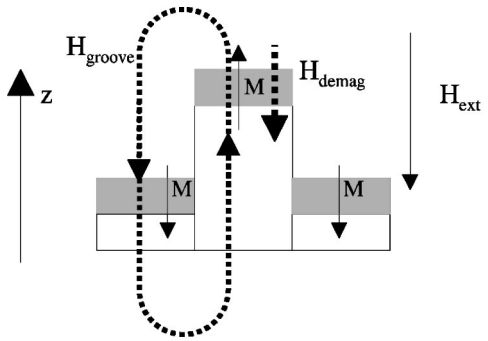


FIG. 14. Schematic representation of the various fields acting on the dots and considered for the change in coercive field of the whole array.

for this configuration shows that the field variation on this given dot is only of 2 Oe when the size of the dots varies from 400 to 200 nm. Therefore, this first contribution can be neglected. Let us now consider the second and third contributions (Fig. 14). At the coercive field of the dots, the magnetization of the whole groove is uniform and already in the down direction since the coercive field in the grooves is much lower than on the dots (Sec. III). Therefore the groove can be considered as the sum of a continuous layer with a negative uniform magnetization and of an array of dots with a uniform positive magnetization [Fig. 11(b)]. The stray field of this system can be calculated with the same method as presented before. It gives at the center of a dot of height *h* a positive stray field $H_{groove}$, whereas the self-demagnetizing field of the dot $H_{demag}$, as well as the external applied field, gives negative contributions.

Consequently, the variation of the coercive field between two different geometries *i* and *j* is $H^j - H^i = (H^j_{groove} - H^i_{groove}) - (H^j_{demag} - H^i_{demag})$. Table IV shows that a reasonable agreement between experimental and calculated variations is obtained. These results confirm the fact that there is no significant change in the magnetization reversal mechanism in the arrays of dots when their size decreases from 400 nm to 200 nm.

## VIII. CONCLUSIONS

We have shown that the deposition of (Co/Pt) multilayers on patterned silicon substrates can be used to prepare single domain submicronic magnetic dots with enhanced coercivity. This increase is ascribed to the reduced influence of major defects for isolated dots compared to a continuous layer. The negligible amount of magnetic material deposited on the sidewalls of the dots does not induce perturbing effects in the magnetic configurations of the top of the dots. Furthermore,

TABLE IV. Experimental and calculated variations of the coercive field as a function of the geometry of the array.

| Considered arrays | Experimental $\Delta H_c$ (Oe) | Calculated $\Delta H_c$ (Oe) |
|---|---|---|
| $L=400$, $d=100$, $h$ from 47 to 200 | $-85$ | $-26$ |
| $L$ from 400 to 300, $d=100$, $h=47$ | $+31$ | $+39$ |
| $L$ from 400 to 300, $d=100$, $h$ from 200 to 47 | $+116$ | $+65$ |
| $L$ from 400 to 200, $d=100$, $h=200$ | $+62$ | $+67$ |

despite the presence of magnetic material in the grooves, our results show that any magnetic configuration could be stored on these dots, which is of considerable interest for applications to storage media.

Compared to continuous films, the reversal mechanism is unchanged for dots and occurs via nucleation and propagation, as long as the domain wall width is well above the dot size. The distribution of reversal fields cannot be ascribed to magnetostatic interactions between dots. It is associated with the detailed shape of the dots resulting from the patterning process.

Micromagnetic calculations have been carried out by considering both magnetic deposits on top of dots and in the bottom of the grooves. The calculated magnetostatic energy can explain the change in the coercive field of the whole array with the geometry of the dots, and confirms that the reversal mechanism in the dots does not fundamentally change while the dots' size varies from 400 nm to 200 nm. By extrapolating the magnetic calculations to arrays of square dots with a dot size of 30 nm and a spacing of 50 nm (corresponding to a density of 100 Gbit/in.$^2$), the maximum magnetostatic field on a given dot would be 70 Oe. Since the coercive field of the dots increases as their size decreases, these calculations show that the present preparation technique would still be efficient for ultrahigh-density recording media.

## ACKNOWLEDGMENTS

These experiments were performed in the framework of the PLATO program. The authors gratefully acknowledge B. Dal'Zotto, S. Tédesco, and M. Heitzmann (LETI, CEA Grenoble) for the preparation of the patterned silicon substrates.

*Author to whom correspondence should be addressed. Electronic address: slandis@cea.fr

[1] S. Y. Chou, IEEE Trans. Magn. **85**, 652 (1997).
[2] M. Johnson, J. Vac. Sci. Technol. A **16**, 1806 (1998).
[3] G. A. Prinz, Science **282**, 1660 (1998).
[4] T. Aign, P. Meyer, S. Lemerle, J.-P. Jamet, J. Ferré, V. Mathet, C. Chappert, J. Gierak, C. Vieu, F. Rousseaux, H. Launois, and H. Bernas, Phys. Rev. Lett. **81**, 5656 (1998).
[5] S. Y. Chou, P. R. Krauss, and L. Kong, J. Appl. Phys. **79**, 6101 (1996).
[6] J. I. Martin, J. Nogués, I. K. Schuller, M. J. Van Bael, K. Temst, C. Van Haesendonck, V. V. Moshchalkov, and Y. Bruynseraede, Appl. Phys. Lett. **72**, 255 (1998).
[7] E. F. Wassermann, M. Thielen, S. Kirsch, H. Weinforth, and A. Carl, J. Appl. Phys. **83**, 1753 (1998).
[8] M. Hanson, C. Johansson, B. Nilsson, P. Isberg, and R. Wäppling, J. Appl. Phys. **85**, 2793 (1999).
[9] S. Landis, B. Rodmacq, B. Dieny, B. Dal'Zotto, S. Tédesco, and M. Heitzmann, Appl. Phys. Lett. **75**, 2476 (1999).
[10] T. Ono, Y. Sugita, K. Shigeto, K. Mibu, N. Hosoito, and T. Shinjo, Phys. Rev. B **55**, 14 457 (1997).
[11] A. Sugawara, T. Coyle, G. G. Hembree, and M. R. Scheinfein, Appl. Phys. Lett. **70**, 1043 (1997).
[12] S. Gadetsky, J. K. Erwin, M. Mansuripur, and T. Suzuki, J. Appl. Phys. **79**, 5687 (1996).
[13] S. Hashimoto, Y. Ochiai, and K. Aso, J. Appl. Phys. **66**, 4909 (1989).
[14] Z. Zhang, P. E. Wigen, and S. S. P. Parkin, J. Appl. Phys. **69**, 5649 (1991).
[15] Z. G. Li, P. F. Garcia, and Y. Cheng, J. Appl. Phys. **73**, 2433 (1993).
[16] C. L. Canedy, X. W. Li, and Gang Xiao, J. Appl. Phys. **81**, 5367 (1997).
[17] S. Zhang, Phys. Rev. B **51**, 3632 (1995).
[18] J. Pommier, P. Meyer, G. Pénissard, J. Ferré, P. Bruno, and D. Renard, Phys. Rev. Lett. **65**, 2054 (1990).
[19] S. Honda, Y. Ikegawa, and T. Kusuda, J. Magn. Magn. Mater. **111**, 273 (1992).
[20] B. Kaplan and G. A. Gehring, J. Magn. Magn. Mater. **128**, 111 (1993).
[21] M. Kleiber, F. Kümmerlen, M. Löhndorf, A. Wadas, D. Weiss, and R. Wiesendanger, Phys. Rev. B **58**, 5563 (1998).
[22] L. Kong, L. Zhuang, and S. Y. Chou, IEEE Trans. Magn. **33**, 3019 (1997).
[23] T. G. Pokhil, J. Appl. Phys. **81**, 5035 (1997).
[24] M. Hehn, K. Ounadjela, J.-P. Bucher, F. Rousseaux, D. Decanini, B. Bartenlian, and C. Chappert, Science **272**, 1782 (1996).
[25] N. Bardou, B. Bartenlian, C. Chappert, R. Mégy, P. Veillet, J.-P. Renard, F. Rousseaux, M.-F. Ravet, J.-P. Jamet, and P. Meyer, J. Appl. Phys. **79**, 5848 (1996).
[26] J.-P. Jamet, S. Lemerle, P. Meyer, J. Ferré, B. Bartenlian, N. Bardou, C. Chappert, P. Veillet, F. Rousseaux, D. Decanini, and H. Launois, Phys. Rev. B **57**, 14 320 (1998).
[27] W. Rave, K. Fabian, and A. Hubert, J. Magn. Magn. Mater. **190**, 332 (1998).
[28] D. G. Streblechenko, M. R. Scheinfein, M. Mankos, and K. Babcock, IEEE Trans. Magn. **32**, 4124 (1996).
[29] O. Fruchart, J.-P. Nozières, W. Wernsdorfer, and D. Givord, Phys. Rev. Lett. **82**, 1305 (1999).
[30] M. Thielen, S. Kirsch, H. Weinforth, A. Carl, and E. F. Wasserman, IEEE Trans. Magn. **34**, 1009 (1998).
[31] C. Haginoya, K. Koike, Y. Hirayama, J. Yamamoto, M. Ishibashi, O. Kitakami, and Y. Shimada, Appl. Phys. Lett. **75**, 3159 (1999).
[32] F. Fournel, Y. Chen, F. Carcenac, N. Essaidi, H. Launois, V. Kottler, and C. Chappert, IEEE Trans. Magn. **34**, 1027 (1998).
[33] J. F. Smyth, S. Schultz, D. R. Fredkin, D. P. Kern, S. A. Rishton, H. Schmid, M. Cali, and T. R. Koehler, J. Appl. Phys. **69**, 5262 (1991).
[34] K. Y. Guslienko, Appl. Phys. Lett. **75**, 394 (1999).
[35] R. L. Stamps and R. E. Camley, Phys. Rev. B **60**, 11 694 (1999).
[36] O. Fruchart, J.-P. Nozières, B. Kevorkian, J.-C. Toussaint, D. Givord, F. Rousseaux, D. Decanini, and F. Carcenac, Phys. Rev. B **57**, 2596 (1998).
[37] C.-R. Chang and J.-S. Yang, IEEE Trans. Magn. **32**, 714 (1996).
[38] J.-S. Yang, J. Lee, and C.-R. Chang, IEEE Trans. Magn. **34**, 2469 (1998).